Three-dimensional hydrostratigraphical modelling supporting the evaluation of fluoride enrichment in groundwater: Lakes basin (Central Ethiopia)

Giorgio Ghiglieri [a,*], Marco Pistis [a], Bekele Abebe [b], Tilahun Azagegn [b], Tesfaye Asresahagne Engidasew [c], Daniele Pittalis [d], Albert Soler [d], Manuela Barbieri [d], Didac Navarro-Ciurana [d], Raúl Carrey [d], Roger Puig [d], Alberto Carletti [e,f], Roberto Balia [g], Tigistu Haile [b]

[a] *Department of Chemical and Geological Science, University of Cagliari, Cittadella Universitaria di Monserrato, Blocco A – S.P. Monserrato-Sestu, km 0.700, Italy*
[b] *School of Earth Sciences, Addis Ababa University, College of Natural Sciences, P.O. Box 1176, Addis Ababa, Ethiopia*
[c] *GEOMATRIX, Around Megenagna, Woreda 6, Bole Subcity, Addis Ababa, Ethiopia*
[d] *Grup MAiMA, SGR Mineralogia Aplicada, Geoquímica i Geomicrobiologia, Departament de Mineralogia, Petrologia i Geologia Aplicada, Facultat de Ciències de la Terra, Universitat de Barcelona (UB), C/ Martí i Franquès, s/n, 08028 Barcelona, Spain*
[e] *Desertification Research Group (NRD), University of Sassari, Viale Italia, 07100 Sassari, Italy*
[f] *Department of Agriculture, University of Sassari, Viale Italia 39, 07100 Sassari, Italy*
[g] *Department of Civil-Environmental Engineering and Architecture, University of Cagliari, Piazza d'Armi, 1, Cagliari 09123, Italy*

A R T I C L E   I N F O

A B S T R A C T

Study region: The Lakes Basin is located in the Main Ethiopian Rift. It covers the northern part of the rift valley basin, the Upper Awash River basin, and some sub-basins from the Omo River basin. Due to the presence of high fluoride (F^-) content, natural contamination of groundwater has long been recognized as a water-related health issue in the area.

Study focus: A multidisciplinary research effort, including geological, hydrogeological, hydrochemical, and geophysical investigations, was adopted to understand the 3D hydrogeological conceptual model and to evaluate F^- enrichment in groundwater.

New hydrological insights for the region: The 3D hydrogeological conceptual model shows a complex hydrogeological environment and a clear hydraulic interconnection between different aquifers. The geological setting has deeply influenced the geometry of the aquifers, recharge and discharge areas, and F^- enrichment in groundwater. Two hydrogeological units, namely sedimentary and volcanic multi-aquifers, were identified. The analyses of groundwater circulation, flow paths, and distribution of F- concentrations in each aquifer were conducted. In groundwater, the concentration of fluoride varies from 0.1 to 68.9 mg L^{-1}; in surface water, it ranges from 0.6 to 244.2 mg L^{-1}. Fluoride concentration of 62 % of the water samples analyzed exceeded the 1.5 mg L^{-1} WHO threshold for fluoride concentration in drinking water. The proposed methodological approach has been demonstrated to be a powerful tool that could be applied in other similar areas.

* Corresponding author.
   E-mail address: ghiglieri@unica.it (G. Ghiglieri).

1. Introduction

At least 44 % of the population in sub-Saharan Africa (approximately 320 million people) do not have access to clean and reliable water supplies (JMP, 2004; MacDonald et al., 2008; Ghiglieri and Carletti, 2010). The majority of those without access to clean water (approximately 85 %) live in rural areas where the consequent poverty and ill health severely affect women and children (JMP, 2004; MacDonald et al., 2008). In these areas, groundwater plays a central role (Pietersen, 2005; Davies, 2008). The unregulated and rapidly increasing groundwater exploitation is one of the major problems in water resources management (Ghiglieri and Carletti, 2010). In addition, the problem is exacerbated by natural water contamination due to high fluoride (F^-) content (Alemayehu, 2010; Ghiglieri et al., 2010 and 2012; Ayenew, 2018). Some of the highest fluoride contents in groundwater ever recorded in the world have been found in the East African Rift System (EARS) with the concentrations of up to 68.9 mg L^{-1} in Ethiopia, and even more than 100 mg L^{-1} in Tanzania (Alemayehu, 2010; Mckenzie et al., 2010). For this reason, fluoride has long been recognized as a water-related health concern in Ethiopia. Fluoride problems are largely found in groundwater from active volcanic zones, where fluorine is derived from volcanic rocks and associated geothermal activities (Alemayehu, 2010; Ghiglieri et al., 2010 and 2012; Ayenew, 2018). These high fluoride contents are ascribed to geological processes, including thermal springs, groundwater flow through rocks with fluorite and apatite minerals, and volcanic activity (Ghiglieri et al., 2012). Delcamp et al. (2016) reported various water evolutionary trends in volcanic aquifers. They emphasize that many changes in hydrogeological conditions strongly influence fluoride dynamics for a mature volcano.

It is reasonable to first address the geochemical association of F^- with the hydrogeological and geological setting. To understand these dynamics and prior to the development of groundwater facilities, the capability of project should be confirmed through a hydrogeological conceptual model of the area, based on geological information, geophysical data, aquifer, and hydrogeochemical properties (Xue et al., 2004; Tam et al., 2014). During the last few years, the techniques in three-dimensional (3D) hydrogeological model reconstruction and visualization have been tested and applied as an effective approach (Ghiglieri et al., 2016 and references therein; Butscher et al., 2017), combining different datasets (e.g., geological, hydrogeological, and geophysical). The thickness, depth, lateral facies extent, stratigraphy, and geometry of aquifers can be exhibited using 3D visualization software to produce block diagrams and slice maps. This offers a better and more reliable picture of the subsurface geology, which can define the hydrogeological conceptual models and understanding of groundwater dynamics.

This study explores a robust 3D modeling method that processes sub-surface geology assessment, borehole, geophysical, and hydrochemical data, and considers the influence of missing information. The remainder of this paper is organized as follows. The structural characteristics of the volcano-sedimentary stratigraphic system are summarized in Section 2, which also considers the structural framework. Section 3 introduces the modeling methodology and a novel implementation approach. Section 3 also concentrates on the major steps and technical details of the method. In Section 4, the feasibility of the above methodological approach in understanding F^- enrichment in groundwater is demonstrated. The conclusions of this study are provided in Section 5. In developing countries, the proposed approach would also be useful in the case of data collection difficulties and in developing efficient management strategies to improve water quality and resource availability. The study was carried out within the framework of the Horizon 2020 interdisciplinary FLOWERED Project (de-FLuoridation technologies for imprOving quality of WatEr and agRo-animal products along the East African Rift Valley in the context of aDaptation to climate change; www.floweredproject.com).

2. Description of the study area

2.1. Geographic, climatic, and physiographic setting

The study area is located in the Main Ethiopian Rift (MER) and extends between latitudes 6°50′N and 8°37′N and longitudes 38°27′E and 39°40′E (Fig. 1). It covers a rhomboidal area of approximately 30,000 km^2, where the elevation ranges between 1600 and 2500 m above sea level. It covers the northern part of the rift valley basin, the Upper Awash River basin, and some sub-basins from the Omo River basin. More specifically, in this work, the Lake Ziway area has been selected for comprehensive studies, as it is characterized by the most interesting hydrogeological and hydrochemical features within the overall study area as well as the availability of an already existing comprehensive dataset. The Lake Ziway watershed covers approximately 7300 km^2, including the Rift Valley floor, the escarpment areas, two major river inlets (Ketar and Meki rivers), and one river outlet (Bulbula River). The area can be divided into three physiographic zones: the rift, transitional escarpments, and rift shoulders. The topography of the area is strongly controlled by geology (volcanism and faulting) and erosion. The MER is a broad depression bounded by discontinuous border faults. Tectonics and volcanic activities became restricted to the narrow axial zone during the Quaternary (Boccaletti et al., 1999), giving rise to grabens, half grabens, and horsts (Corti, 2009, 2012). This morphology provides suitable pathway for the circulation and storage of surface water and groundwater fed by numerous rivers flowing towards the rift floor. There are also numerous perennial streams, restricted to the rift valley, the largest being the Awash River. All rift lakes receive recharge from both rain and groundwater, whereas some lakes such as Abijata and Shalla do not have groundwater outflow (Alemayehu et al., 2006; Kebede et al., 2008). The rift is also characterized by wetlands that are sustained by groundwater (Alemayehu, 2010). The climate is warm, and precipitation mostly occurs during summer and persists from mid-June to mid-September, whereas scanty rainfall may also occur during March, April, and May. The average annual temperature is 19.3 °C in Ziway, with an annual average rainfall of 837 mm (Alemayehu, 2010). The driest month is December, with precipitation going as low as 6 mm. In the region, the water most commonly used by residents for drinking and domestic use is that from springs and wells.
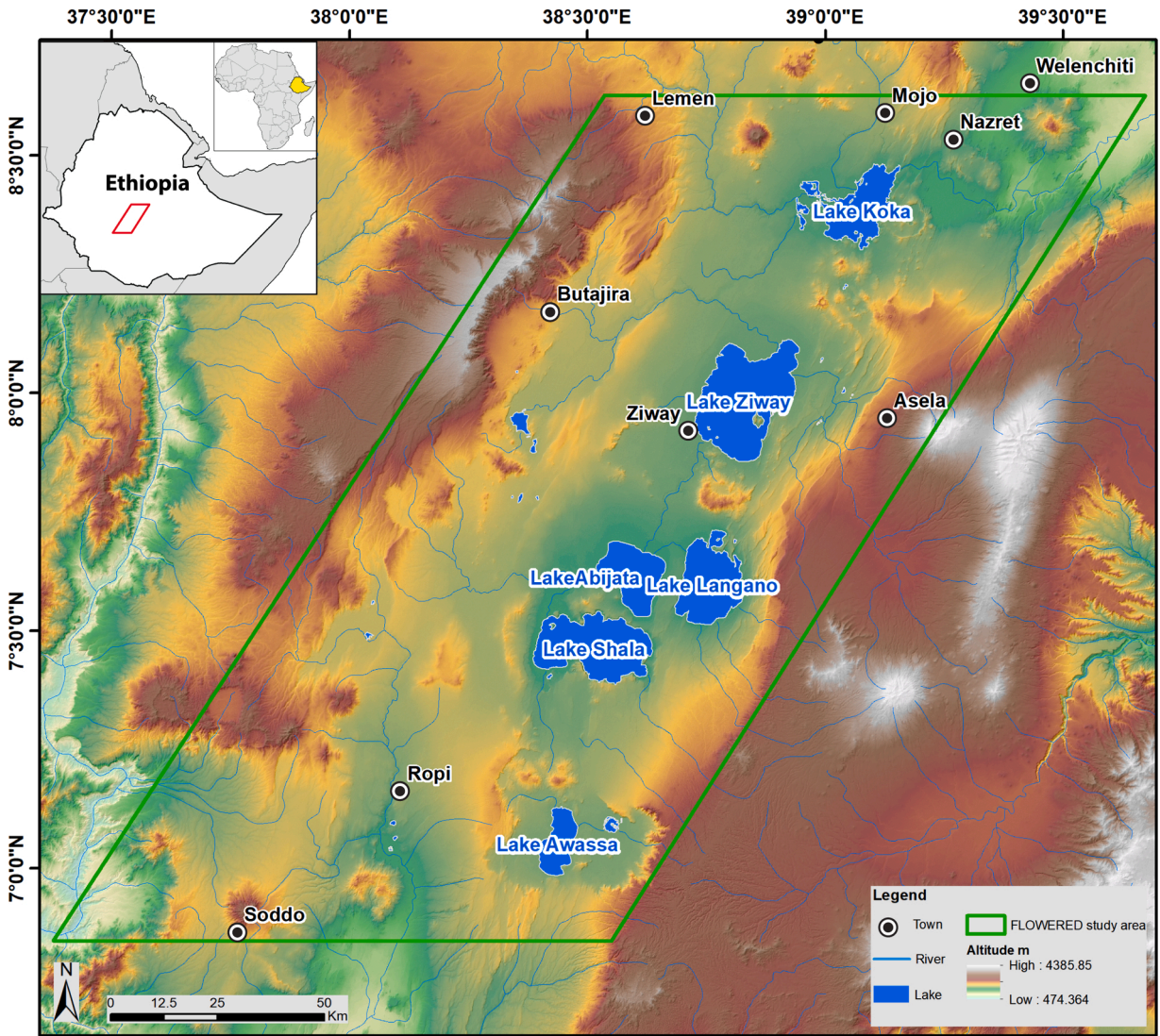
Fig. 1. Central Main Ethiopian Rift (the dark line marks the study area).

2.2. Geological and hydrogeological setting

The rift is bordered by the escarpments that separate its floor from the adjacent plateaus. The rift floor hosts several lakes, volcanoes, and calderas. The development of the EARS in Ethiopia began with the eruption of continental flood basins between 30 and 29 My (Wolfenden et al., 2004), followed by faulting in the north and south, which propagated towards the central part of the rift. This major tectono-magmatic event, which altered the configuration of the landscape, has also entirely changed the region's hydrological setting.

The study area is almost exclusively covered by acid to basic volcanic rocks, lacustrine, and alluvial sediments. Quaternary lacustrine and alluvial sediments occupy the low-lying flat to gently sloping grabens and half grabens. Late Pliocene and Quaternary volcanic rocks dominate the escarpment zone and low-lying rift (Wolde Gabriel et al., 1990; Abebe et al., 2007). Quaternary acidic centers erupted pyroclastic products and lavas, located mainly along the active rift axis named the "Wonji Fault Belt" (Kebede et al., 2008); associated with those, localized basaltic flows and aligned monogenetic basaltic cones are observed (Trippanera et al., 2015). Precambrian and Mesozoic rocks are locally exposed in the Kella area (western margin) under a thick Oligocene and Pliocene volcanic rocks sequence. The main aquifer systems are typically fractured and/or weathered volcanics, or weathered contact zones between different lithological units; these aquifers are often confined or semi-confined. Aquifers with relatively high permeability are found in
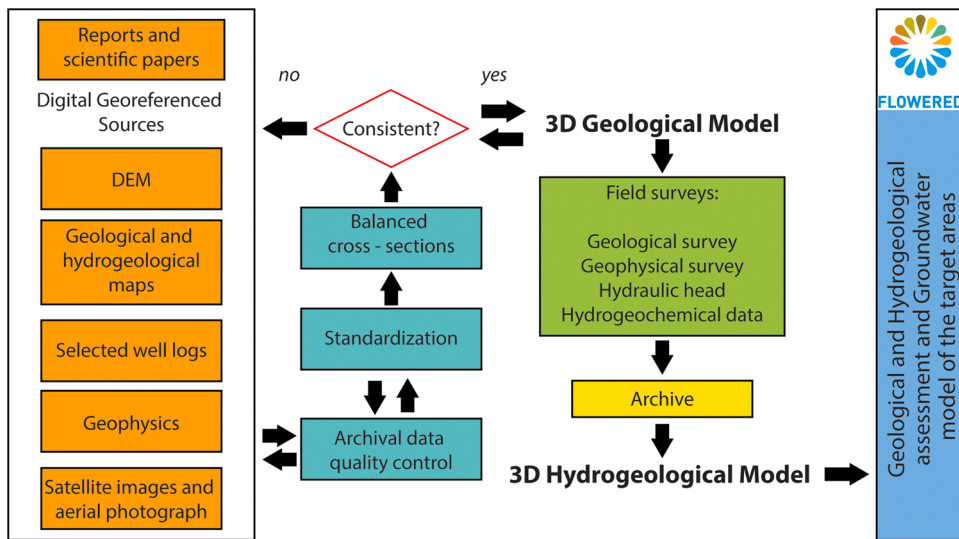
Fig. 2. Flowchart for methodology of 3D hydrogeological model building.

sediments, covering parts of the rift floor. The permeability of rocks in the MER is medium (4×10^{-4} ms^{-1}), although there is considerable local variation (Alemayehu, 2010). Indeed, geological events have deeply influenced the geometry of the aquifers, recharge and discharge areas, and groundwater quality. Rocks are laterally discontinuous, aquifer composition is heterogeneous, and aquifer hydrodynamic characteristics are variable (Kebede et al., 2008). Therefore, the connection between the volcanic, volcano-lacustrine, and alluvial aquifers, along with volcanic highland aquifers pose significant challenges because of the complex nature of groundwater flow, recharge, and geochemical evolution in these aquifers due to the presence of faults and volcanic activity.

Geothermal activity is manifested by the occurrence of hot springs, fumaroles, boiling pools, hot and steaming grounds, closely associated with Quaternary volcanoes in the axis of the rift (Ayenew, 2008). Hot springs also occur on the flanks of the rift, where they are associated with peripheral faults. As reported by Ayenew (2008), the volcanic centers are characterized by geothermal manifestations and are aligned along the tectonically active fault system called the Wonji Fault Belt (WFB).

3. Material and methods

Literature review and direct field surveys are the input data sources for the present research. Fig. 2 reports the conceptual workflow of the methodological approach developed herein, according to a method already applied in previous research (Ghiglieri et al., 2016; Dodagoudar, 2018) and used for the construction of the geological and hydrogeological 3D model and to understand F$^-$ enrichment in groundwater. Literature data (e.g., papers, reports, and maps) were verified and homogenized (the consulted data are different in terms of nomenclature, colors, and degree of differentiation of the lithological units, geological, stratigraphic, tectonics, hydrogeology, and so on), and then loaded into the database. Field surveys were performed to acquire new datasets using a multidisciplinary approach, integrating geology, geophysics, hydrogeology, hydrochemistry, and isotopes.

3.1. Stratigraphic analysis, geological cross-sections, and data handling

Preliminary geological information was obtained from previous studies (Geological map of the northern Main Ethiopian Rift, scale 1:200.000; Abebe et al., 2005) whereas detailed mapping has been carried out during the present research (Fig. 3). Stratigraphic data have been gathered from stratigraphic well-logs, papers (Abebe et al., 2005; Agostini et al., 2011) or previous projects and unpublished work. A great effort was made to homogenize all the geological, stratigraphic, and tectonic information and to convert the data into hydrogeological features. As a second step, several geological sections were constructed and the area around Lake Ziway was selected for the 3D hydrogeological model as it represents one of the most interesting hydrogeological and hydrochemical features in the study area. Six geological cross-sections, selected from a set of twelve, drawn at 1:200.000 scale, were used for the reconstruction of the geological model, and three of them ran perpendicular to the rift axis, whereas the remaining three runs parallel: two cross-rift sections (AA' and BB') extend from the western rift shoulder to the eastern one, whereas the MM' section ends at the center. The three cross-sections parallel to the rift axis run in the rift center (FF' and DD') and in the eastern shoulder (BB'), respectively (Fig. 3).

The geographic information system (GIS) geodatabase was populated with all these data. An ArcGis tool (ArcGis eXacto Section
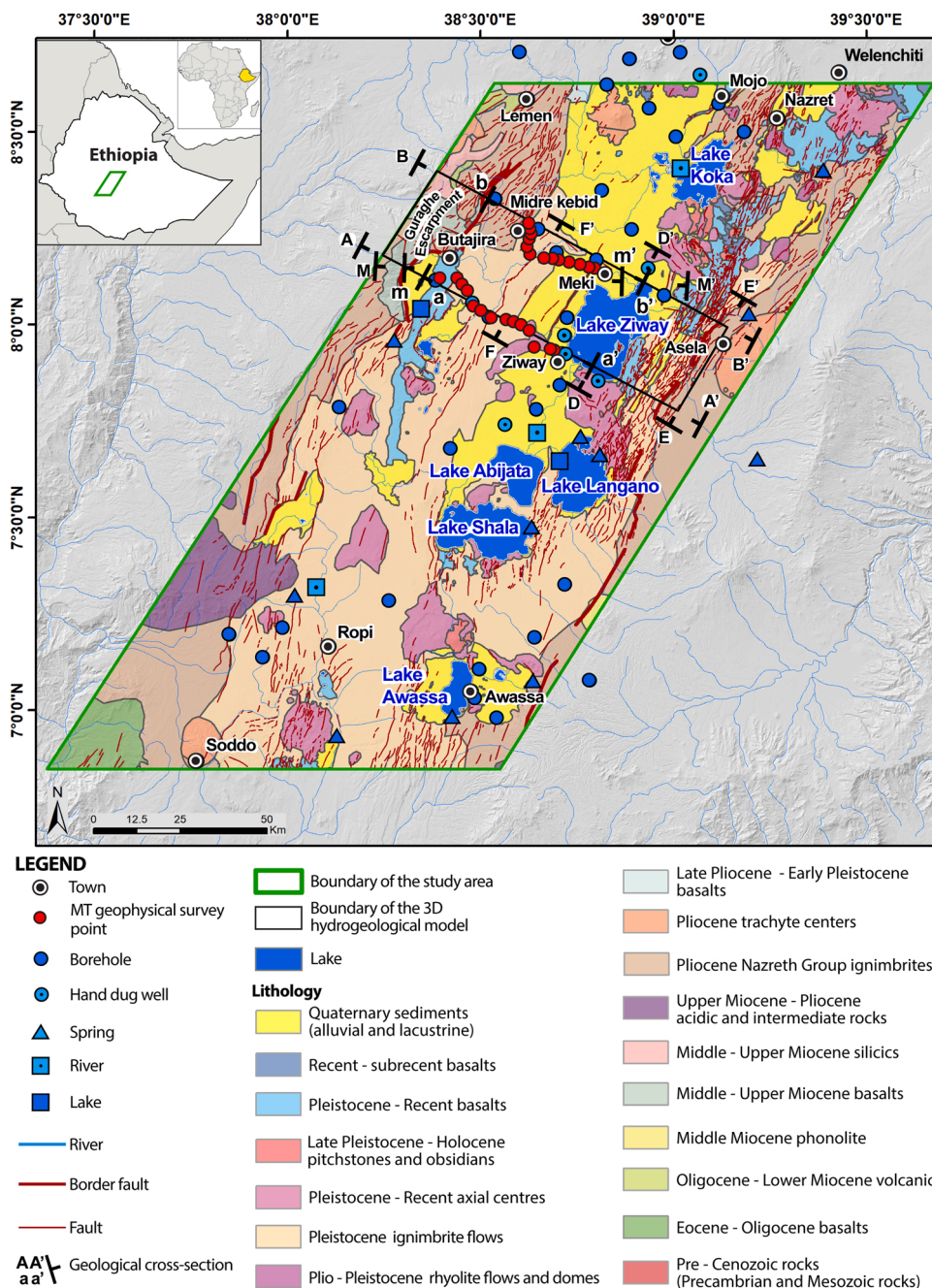
Fig. 3. Geological-hydrogeological map of the study area. Geological cross–sections lines, geophysical survey points (CSA-MT: Controlled Source Audio Magnetotelluric deep soundings) and water sampling points. 3D hydrogeological model domain is also shown.

v2.0), developed by the Illinois State (USA) Geological Survey, was used to process each geological cross-section. The "MOVE" software package (www.mve.com/software/move) was used to verify the 3D consistency of the geological model. It provides a powerful platform for data integration, cross-section construction, and 3D model building. Each geological surface was modeled by the interpolation of the contour lines (depths) drawn, considering the geological cross-sections, stratigraphic data, and interpreted geophysical data.

3.2. Field surveys

To supplement the data acquisition and interpretation described in the previous section, geological, geophysical, hydrogeological,

and hydrochemical surveys were planned and executed.

3.2.1. Geophysical survey

To better constrain the 3D geological model, geophysical measurements, such as classical electrical soundings (VES, Schlumberger spread) and controlled source audio magnetotelluric deep soundings (CSAMT), were carried out along two traverses: the Ziway–Butajira traverse on the southwest and the Meki–Midrekebid traverse on the northeast, as shown in Fig. 3. These traverses follow the major access roads and cross the western side of the rift, from the escarpment to the rift floor. An average sounding interval of 3 km was employed, and each traverse was composed of two lines designated as Line 1 (on the southeast) and Line 2 (on the northwest). The electrical soundings were carried out with a maximum half-current electrode spacing (AB/2) of 1000 m, and in the CSAMT, electromagnetic sounding frequencies of 0.1–1000 Hz were employed. However, we noticed that the resistivity pseudo-sections obtained through the AMT surveys are undoubtedly better than those obtained with the vertical electrical soundings and are more useful in the current work due to their greater depth of investigation. Therefore, the whole interpretation was performed only based on the AMT data.

3.2.2. Hydrogeological and Hydrochemical data collection

The selection of the water points of interest was carried out according to the following criteria: i) complete knowledge of the water points in terms of previous chemistry, stratigraphic, and hydrogeological information (considering the fluoride values, aquifer material, depth of wells, and water temperature); ii) wells containing at least the stratigraphic description; iii) homogeneous geographic distribution of water points; and iv) significant differences among various aquifers. Two sampling field surveys were conducted along MER. To observe the potential seasonal chemical variations and the recharge water influence, the 1st campaign was conducted during the dry season, and the 2nd just after the rainy season. The 1st survey included 56 water sampling points, namely, 34 boreholes, 6 hand-dug wells, 11 springs, 3 rivers, and 2 lakes (Fig. 3). The 2nd field survey was carried out along 47 of the 56 water points identified during the 1st campaign. Three additional points (1 hand-dug well and 2 lakes) were sampled as new water points, leading to a total of 50 water points (27 boreholes, 5 hand-dug wells, 11 springs, 3 rivers, and 4 lakes) for the 2nd field survey.

Constructive and technical data of each well were acquired at each water point location, elevation, and geographical coordinates (using a differential global positioning system, www.trimble.com). Moreover, in situ measurements of physicochemical parameters (pH, temperature, electrical conductivity, and redox potential) were performed using a HACH HQ40D multiparameter device. Water samples were collected for the analysis of fluoride and analyzed at the laboratory of the University of Barcelona using a Thermo Fisher Scientific Orion High performance ion selective electrode 9609BNWP. The precision of the analysis, defined as the standard deviation ($\pm 1\sigma$) of the corrected concentration measured in duplicate samples, was better than 1 %.

4. Results and discussion

4.1. Structural and geological setting

The MER constitutes the northern part of the EARS, connecting the Kenyan Rift with the Afar depression. The MER started to develop during the Miocene period (Davidson and Rex, 1980; Wolde Gabriel et al., 1990). During the Pliocene and Quaternary, it progressively deepened and faulted, and magmatism became more confined to the narrow rift axis. This rift segment is bounded by discontinuous border faults striking between NNE–SSW in the south and NE–SW in the north (Korme et al., 2004). The axial rift zone, which developed in the Quaternary, is dominated by dense, N–S to NNE–SSW striking faults. Volcanism is characterized by bimodal-basalt–rhyolite association with localized occurrences of intermediate rocks; however, the volume of acidic rocks in the area significantly exceeds that of the basaltic rocks. The rift is dominated by acidic centers with associated lava flows and pyroclastic deposits as well as subordinate basalts erupted from fissures and monogenetic events.

In the geo-hydrogeological map of the study area (Fig. 3), the oldest unit is represented by a small sliver of Precambrian rocks overlain by Mesozoic sediments, north of Butajira. Eocene–Oligocene continental flood basalts related to the rift initiation are exposed in the southwestern part of the area. Mid-Upper Miocene silicic rocks and basalts lie over older rocks on the western rift margin. Acidic and trachytic volcanic centers of the Upper Miocene–Pliocene age outcrop on both rift flanks. The Late Pliocene–Pleistocene is dominated by extensive ignimbrite flows and the falls of the Nazreth Group, which cover both the western and eastern escarpments. The exposed thickness of this unit, the basal part consisting of alternating basaltic lava flows and agglomerates, reaches 300 m (Wolde Gabriel et al., 1990). This is overlain by another widespread ignimbrite flow of the Pleistocene age, covering most parts of the rift floor. Small, highly eroded Plio-Pleistocene acidic volcanoes, associated with the Nazreth Group rocks, occur in the northeastern part of the study area. The Pleistocene–Recent rhyolites constitute some of the youngest volcanic products of the study area and consist of rhyolite flows, domes, obsidians, and pitchstones, along with extensive ignimbrites, tuffs, and pumices. They are associated with axial silicic volcanic centers. A close spatial and temporal relationship between these silicic volcanoes and propagating faults, accompanied or followed by basaltic eruptions from fissures and aligned monogenetic cones, suggests that these centers guide deformation and subsequent eruptions (Abebe et al., 2007).

Basaltic lavas, cinder cones, and maars occupy the rift floor and they belong to the Pleistocene–Recent basalts. Their eruption history spans the entire Quaternary period, the youngest radiometric data showing an age of ca. 200 years for basaltic flows (Sieburg et al., 2018). The contemporaneous Butajira volcanic field is restricted to a narrow marginal graben at the base of the western escarpment and is marked by NNE–SSW aligned cinder cones, maars, and some lava aprons. The Quaternary sediment units occupy grabens, half grabens, basal slopes of foot walls of faults, and foot slopes of volcanic ranges. These units consist of alluvial, colluvial,
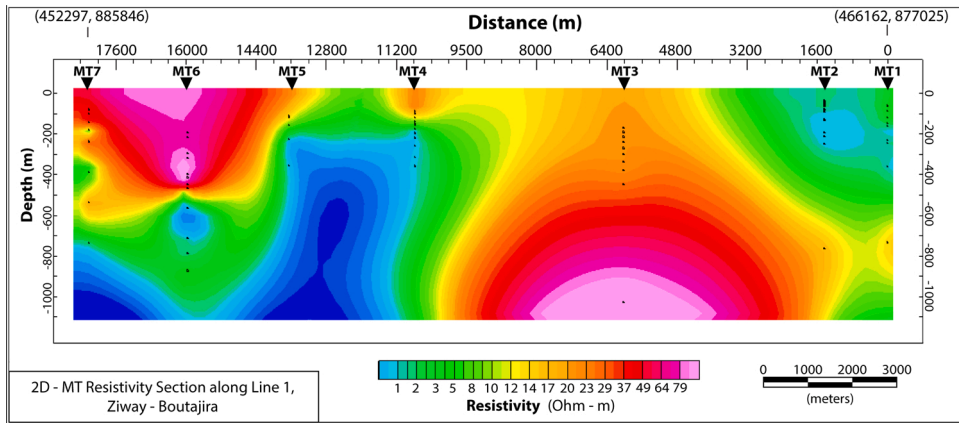
Fig. 4. Line 1 of the Ziway-Butajira transect.

and lacustrine sands and silts, mainly of volcanic origin. Calcrete hardpans, intercalated with these sediments, have significant impacts on water infiltration.

4.2. Geophysical data processing and interpretation

Field data were analyzed, processed, and interpreted to show the results in 2D resistivity sections. First, the geoelectrical sections were evaluated merely in geophysical terms and were then interpreted into geological and hydrogeological terms, considering the knowledge of both surface and subsurface geology.

4.3. Ziway–Butajira- transect: Line 1 and Line 2

As previously reported, the Ziway–Butajira transect is composed of Lines 1 and 2. The resistivity pseudo-section of Line 1 was obtained using seven AMT soundings (MT-1 to MT-7), as shown in Fig. 4. This pseudo-section, and the following ones, show the subsurface apparent resistivity distribution to a depth of 1 km or more.

In the apparent resistivity field of Ziway–Butajira Line 1, two relatively high resistivity areas can be observed, most likely the response of the massive basalt. The first one develops laterally in the region beneath MT-3 for approximately 6 km and down to a depth of at least 1.5 km. The second one develops between MT-5 and MT-7. On the contrary, very low resistivity values were found between MT-4 and MT-5: this zone and the one corresponding to MT-1 and MT-2 could be the response of highly fractured basalt and ignimbrite, saturated with freshwater. The resistivity pseudo-section of Line 2 is associated with the western part of the Ziway–Butajira transect and is oriented in a near E–W direction. The line consists of six MT soundings, MT-8 to MT-13. The pseudo resistivity section AMT data is shown in Fig. 5.

This MT section shows a wide and deep low-resistivity area that extends between MT-10 and the mid-point between MT-11 and MT-12, extends at smaller depths also at the MT-12 and decreases towards MT13. As in the previous case, the low-resistivity anomaly could be very likely associated with a fractured rock volume, hopefully ignimbrites hosting freshwater.
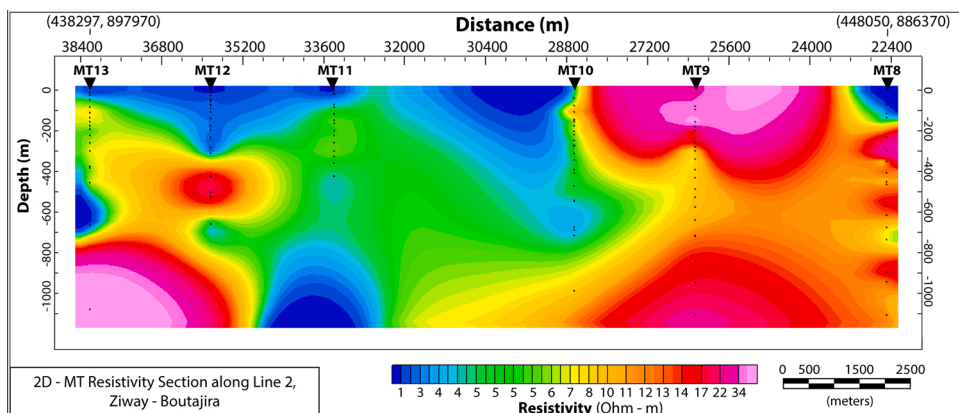

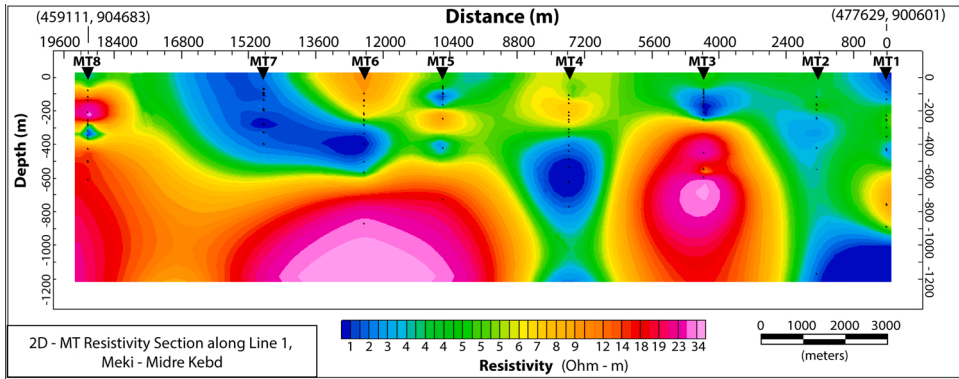**Fig. 5.** Line 2 of the Ziway-Butajira transect.

Fig. 6. Line 1 of the Meki-Midre Kebd transect.

4.4. Meki–Midre Kebd Transect: Line 1 and Line **2**

The Meki–Midre Kebd transect also consists of Line-1 and Line-2. In turn, Line 1 consists of eight MT soundings, starts close to Meki Town and extends westward with an average sounding station spacing of 3 km. The 2D resistivity section is shown in Fig. 6.

Low resistivity can be observed in three areas, namely in the MT-1- MT-3 regions, in depth close to MT-4 and centered in MT-7. Moreover, in this case, low resistivity could be very likely associated with fractured rock volumes, and it is expected that these are ignimbrites that host fresh water.

4.5. Meki–Midre Kebd transect- Line 2

The 2D resistivity section for Line-2 of the Meki–Midre Kebd transect, consisting of sounding MT-8 to MT-13, is shown in Fig. 7. The uppermost low resistivity regions between MT-8 and MT-9, as well as between MT-11 and MT-12, show a response attributable to weathered and fractured ignimbrite, potentially saturated with water.

4.6. Geological cross-sections

Among the twelve geological cross-sections analyzed, six were used to reconstruct the geological model (Fig. 8). The cross-sections perpendicular to the rift axis show horst-graben and half-graben structures. The western highlands (the rift shoulders) are made of the oldest deposits of the pre-rift phase, from Precambrian to Miocene. Subsequently, during the rift phase, they are displaced by the border faults in the main rift, and currently, they are found at different depths, up to a few kilometers low. The syn-rift deposits are represented by the Pliocene Nazret Group ignimbrites, whereas the younger geological formations are located along the rift floor and are dissected by normal faults. A large area of the rift floor is mantled by lacustrine sediments. Among the six sections, three were geophysically interpreted (Fig. 9). In these sections, the low-resistivity volumes are highlighted. As mentioned above, the low resistivity is attributable to weathered and fractured ignimbrite, potentially saturated with water. Moreover, the condition that the extension of the low-resistivity field corresponds to faulting zones (e.g., Abosa Fault) could be associated with deep groundwater circulation.
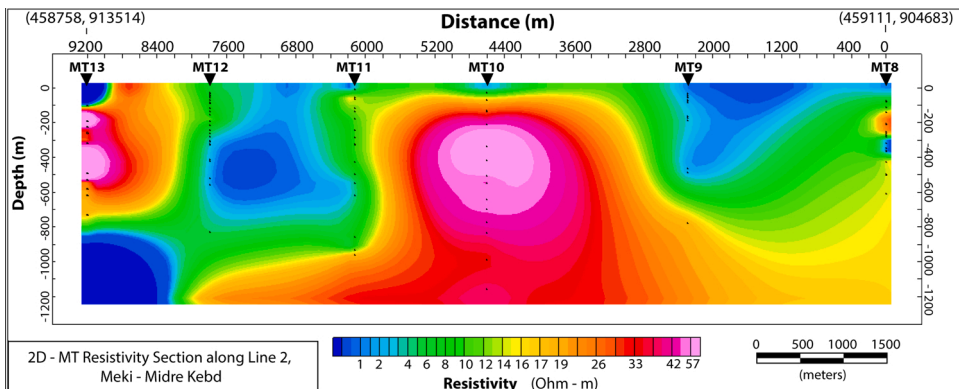

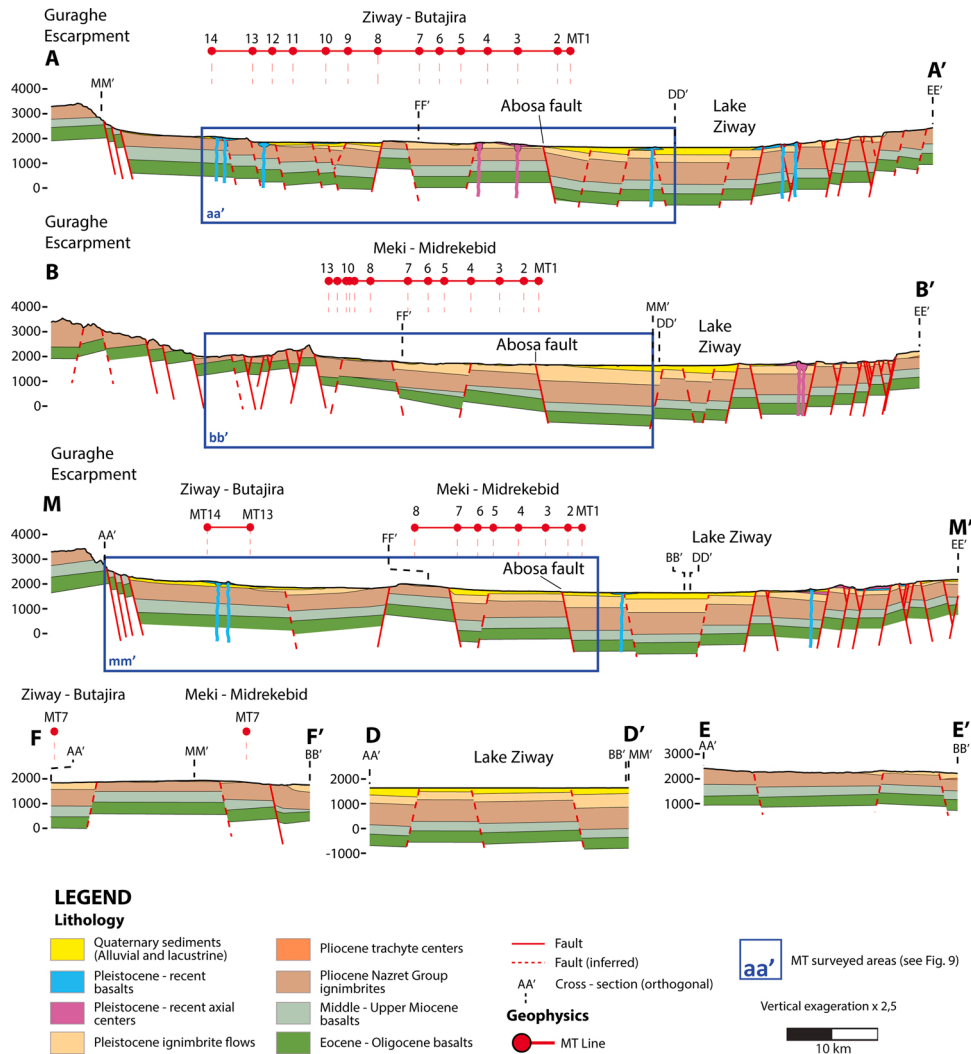**Fig. 7.** Line 2 of the Meki-Midrekebd transect.

Fig. 8. Geological cross-sections. Locations are shown in Fig. 3.

4.7. 3D hydrogeological conceptual model

The 3D model in Fig. 10 has the twin goal of elaborating a local hydrogeological conceptual model and defining the major groundwater flows to predict the diffusion of F^- in the aquifers.

Two hydrogeological units (HU) were identified for the selected area: the sedimentary and volcanic units. The sedimentary aquifer unit consists of aquifers of loose unconsolidated sediments that are mainly composed of lacustrine, alluvial, and volcano-clastic materials. They are moderately productive porous aquifers with transmissivity values ranging from 50 to 10 x $m^2 d^{-1}$ and a well discharge of 2-5 Ls^{-1} (Fentaw and Mihret, 2011). The volcanic aquifer unit, according to Fentaw and Mihret (2011), is represented by five aquifers hosted in five rock units: a) Pleistocene recent basalts having high productivity in fissured rocks with transmissivity ranging from 100 to 500 x $m^2 d^{-1}$ and well discharge of 5–10 Ls^{-1}; b) Pleistocene pyroclastics composed dominantly of pyroclastic fall and ash deposits having low to medium aquifer productivity in fissured and/or porous media, having transmissivity ranging from 1×10 $m^2 d^{-1}$ and well discharge that varies from 0.05–0.5 Ls^{-1}; c) Pliocene fissured ignimbrites moderately productive, having transmissivity values ranging from 50×10 $m^2 d^{-1}$ and a well discharge that varies from 2–5 Ls^{-1}; d) Mid-Upper Miocene basalts and trachybasalts constituting a fissured aquifer of moderate productivity having transmissivity ranging from 50×10 $m^2 d^{-1}$ and well
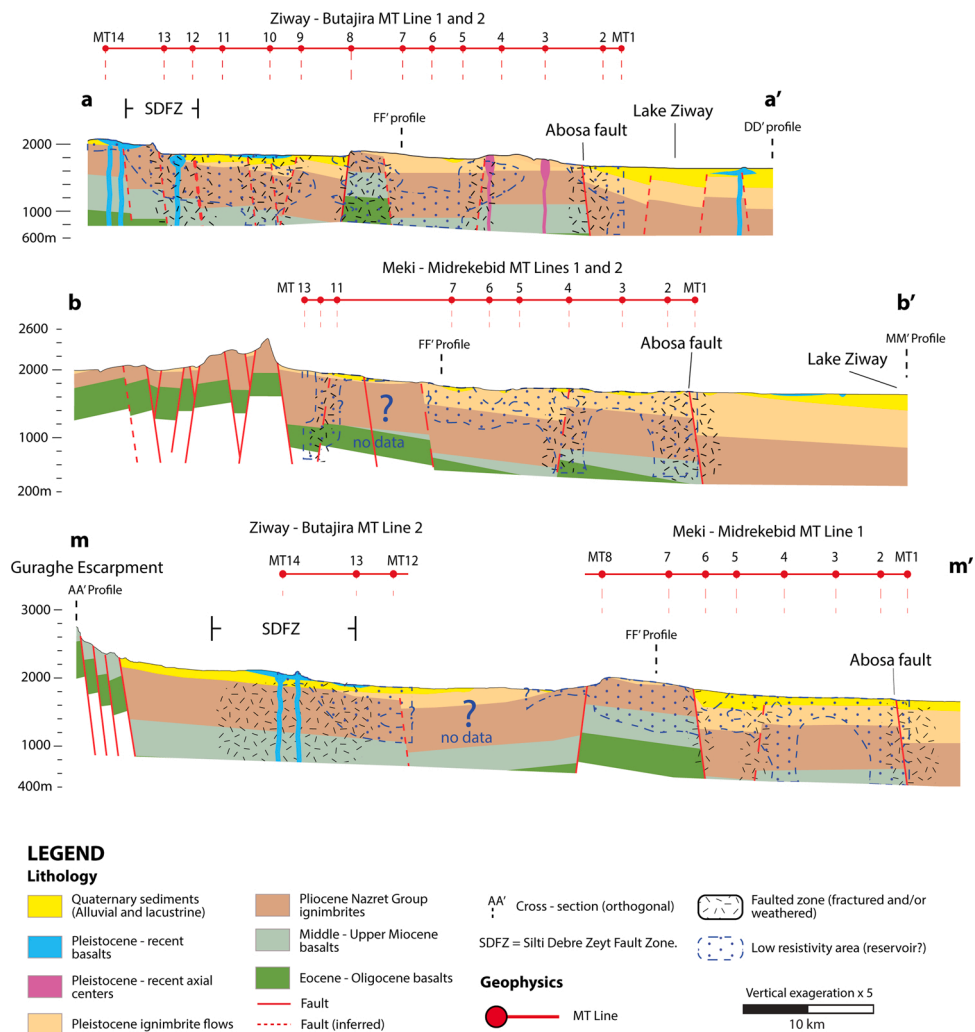
Fig. 9. Geological cross-sections along the MT surveyed areas. Locations are shown in Fig. 3.

discharge varying from 2–5 Ls^{-1}; e) Eocene–Oligocene basalts hosting a moderately productive fissured aquifer with transmissivity of 50×10 m^{2}d^{-1} and a well discharge of 2–5 Ls^{-1}. The 3D hydrogeological model shows the groundwater circulation system (Fig. 10): the main recharge areas are located in the east and west shoulders of the rift; the discharge zones take place in the flanks towards the center of the graben, which is the main groundwater reservoir. The sedimentary aquifer unit is recharged laterally by groundwater flowing from the aquifers hosted in the flanks of the rift. Groundwater sometimes feeds the streams and later infiltrates through channel loss to recharge the aquifers in the transitional slope and in the rift floor. In most parts of the area, shallow aquifers hosted in alluvial sediments are the main groundwater source for water supply through hand-dug wells. Fresh groundwater is also found in basaltic aquifers (Kebede, 2013). Fault zones act as either hydraulic conduits connecting different aquifer systems or form effective barriers to groundwater flow. Because regional fault systems are also present, the groundwater is drained through deep circuits and then rises again in the form of thermal water (Fig. 10).

4.8. Regional groundwater flow

According to Azazegn et al. (2015), differently oriented horsts, caped with impermeable rock units in the western plateau and in the rift margins on the western side of the Northern Main Ethiopian Rift (NMER) define the groundwater divide. The groundwater contribution (inter-basin flow) flows from the surrounding western plateau to the NMER aquifer system (Fig. 11).

The groundwater systems range from the highlands recharge areas in the western, northern, and eastern sides of the rift, to the
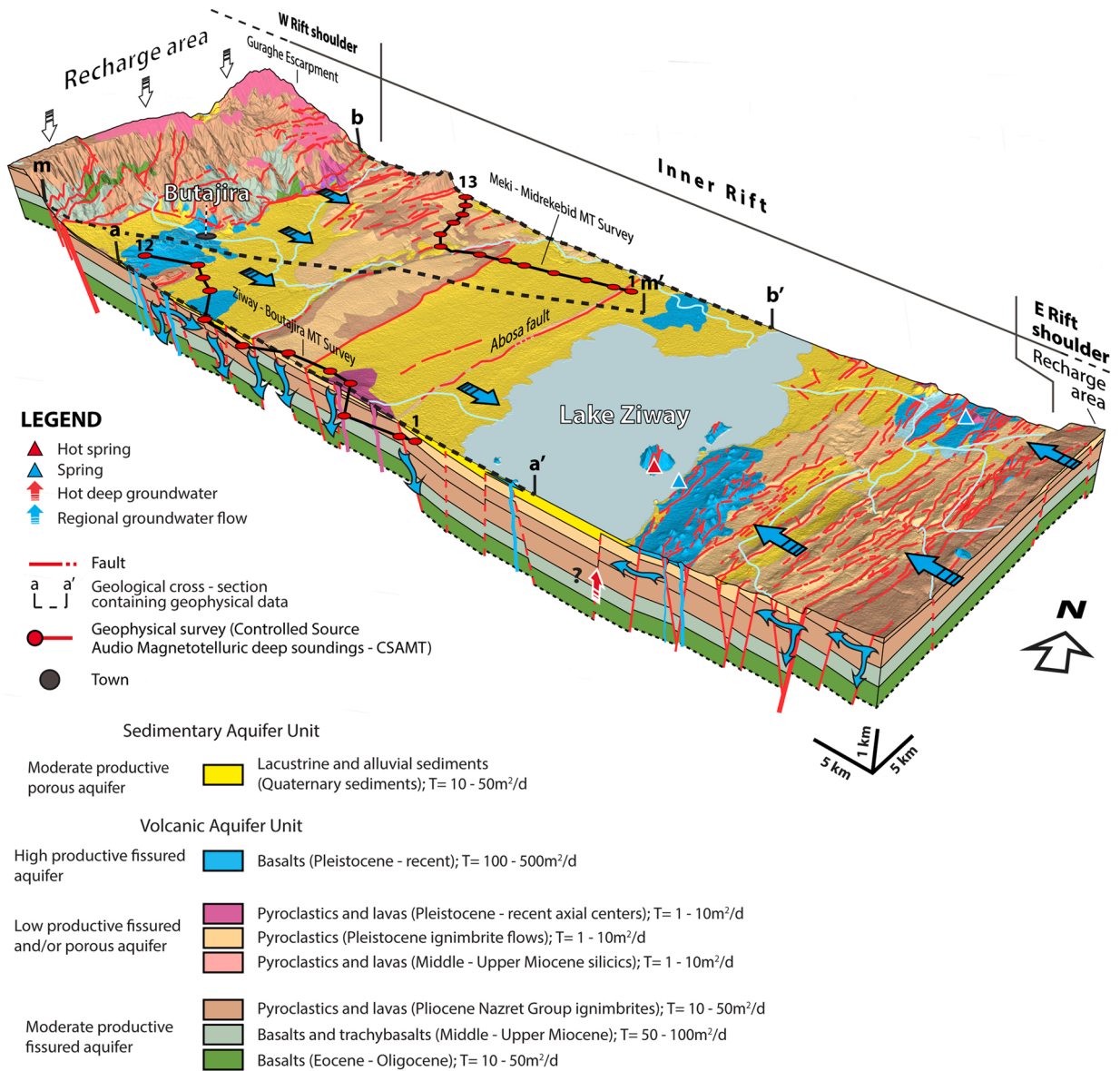
Fig. 10. 3D hydrogeological conceptual model.

lowland discharge areas towards the rift axis, which is, as expected, along the regional slope and depending on the rift structure geometry (Fig. 11).

The study area is divided into three groundwater sub-basins: Awash–Koka, Ziway–Shala, and Awassa–Abaya. The Awash–Koka sub-basin lies on the northern side of the study area. In this sub-basin, groundwater flows towards the east and northeast; the recharge areas are the western and northwestern escarpments, including the surrounding Addis Ababa region, which lies outside the study area. The transfer of groundwater from the Blue Nile basin to this sub-basin has been reported in previous studies (Kebede et al., 2007, Yitbarek et al., 2012, Azagegn et al., 2015). In the Ziway–Shala central sub-basin, groundwater flows towards the lake's region and to the rift axis. The Awassa–Abaya groundwater sub-basin lies in the southern part of the study area. In this sub-basin, groundwater converges from the surrounding escarpments, including the central part of the rift towards Lake Abaya (outside the study area), approximately 100 km south of Lake Awassa.

4.9. Physico-chemical features and fluoride distribution in groundwater

A summary of the values of temperature, electrical conductivity, pH, and redox potential measured in situ at all sampling points is provided in Table 1. The groundwater (GW) samples show a wide temperature range (from 15.3 to 91.8 °C and from 14.3 to 92.1 °C for the 1st and 2nd surveys, respectively), where the highest temperatures correspond to springs and confirm the presence of thermal
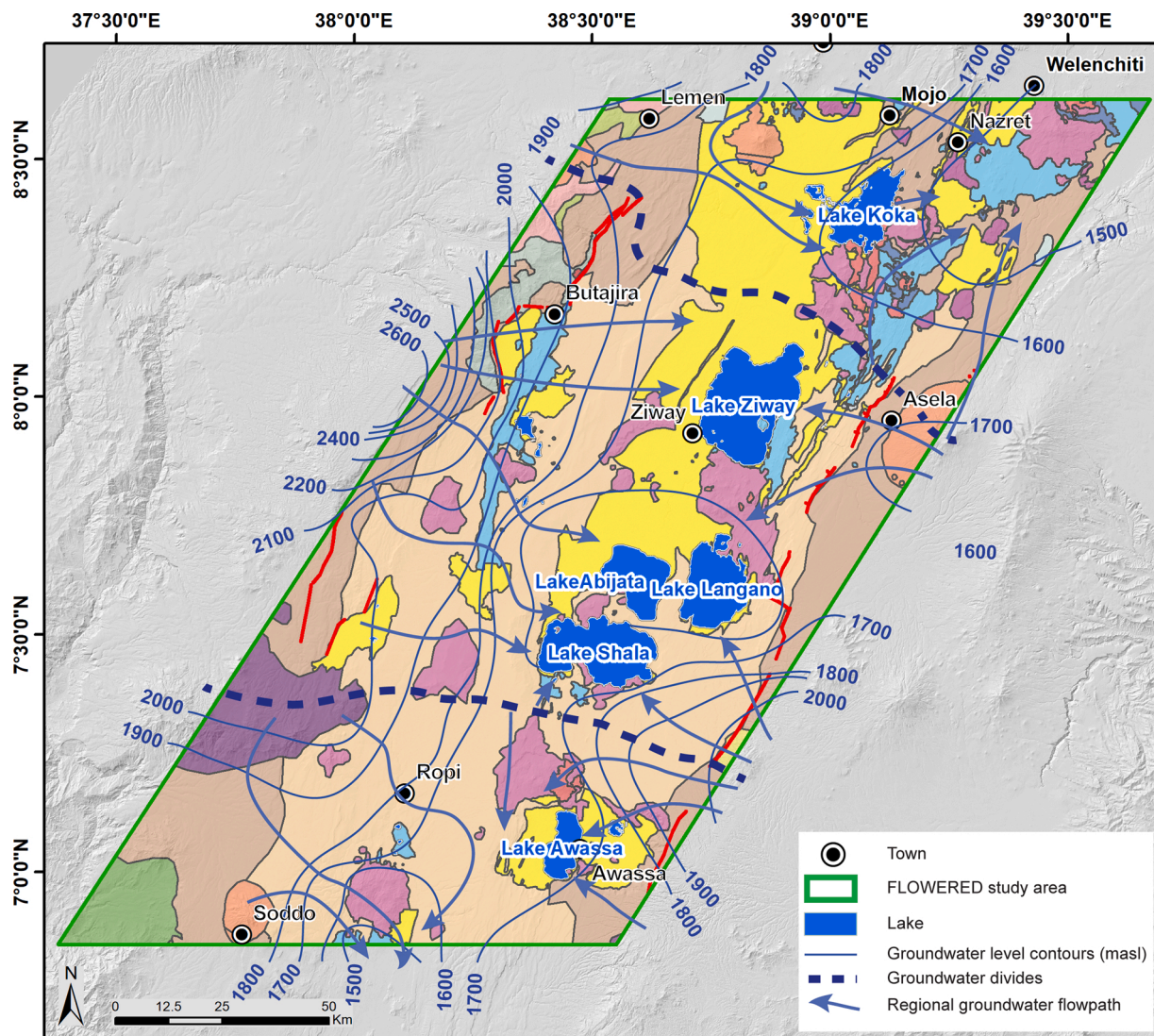
Fig. 11. Groundwater flow pattern of the study area. The elevation is referred in meters above sea level (m a.s.l.). For the geological legend refere to Fig. 3.

Table 1
Summary of the physico-chemical parameters measured in situ at all groundwater (GW) and surface water (SW) sampling points for the 1st and 2nd field survey.

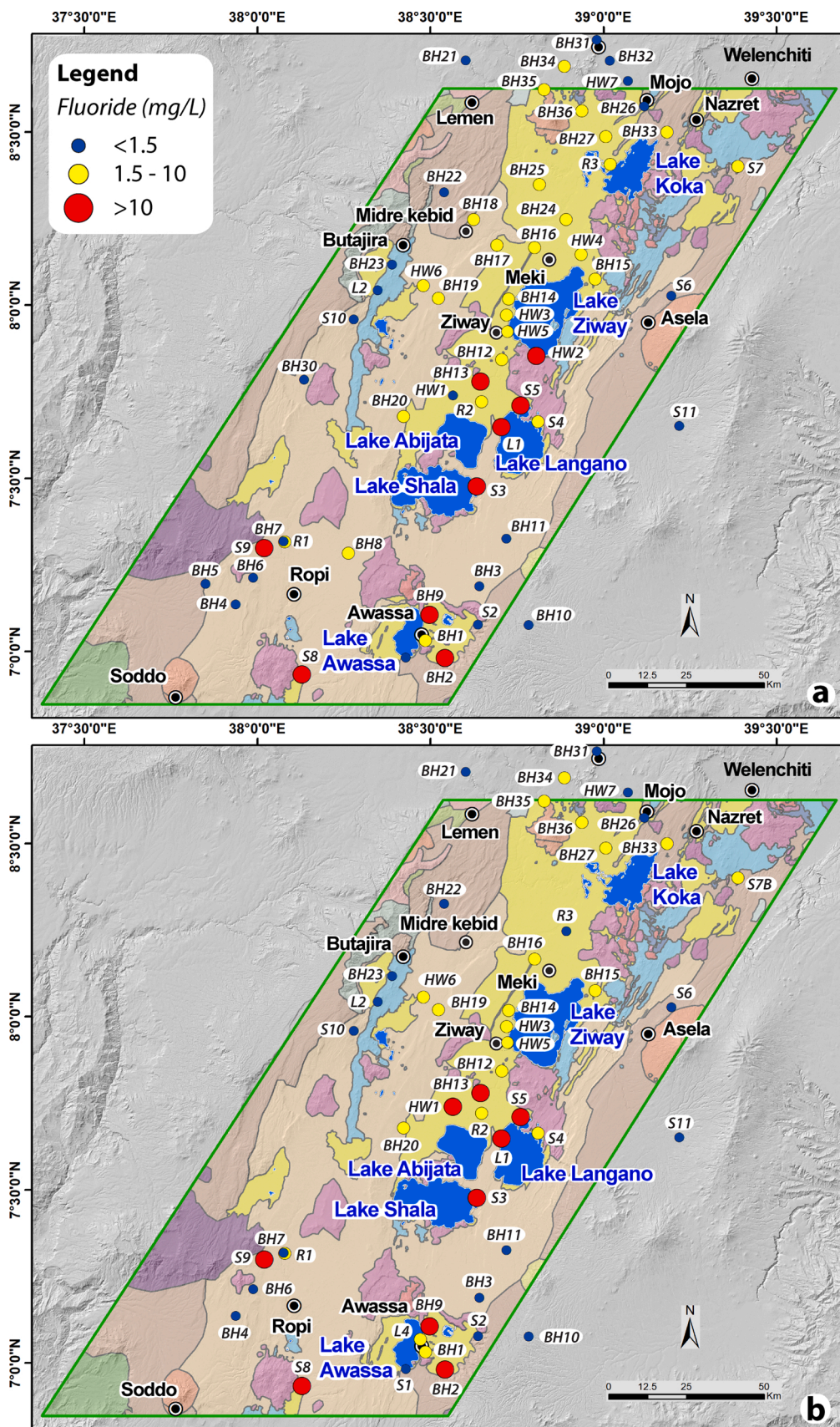|	1st field Survey n = 51 for GW and n = 5 for SW		2nd field Survey n = 43 for GW and n = 7 for SW	
Parameter for GW	Min	Max	Min	Max
pH	6.1	8.9	5.9	9.3
T (°C)	15.3	91.8	14.3	92.1
EC (μScm^{-1})	96	9710	85	5800
Eh (mV)	−287	224	−251	589
Parameter for SW	Min	Max	Min	Max
pH	7.6	8.9	7.6	9.7
T (°C)	18.9	25.9	20.1	26.1
EC (μScm^{-1})	210	1690	89	21,700
Eh (mV)	123	185	113	201

(caption on next page)

Fig. 12. Spatial distribution of fluoride content for the 1st (a) and 2nd (b) field surveys. The symbols not shown in the legend are in Fig. 3.

water. The temperature in surface waters (SW) ranges from 18.9 to 25.9 °C and from 20.1 to 26.1 °C, respectively, for the 1st and 2nd surveys. In GW, the EC varies from 96 µScm^{-1} to 9710 µScm^{-1} for the 1st survey, and from 85 µScm^{-1} to 5800 µScm^{-1} for the 2nd survey, whereas surface waters present a narrower range of conductivities for the 1st survey, from 210 µScm^{-1} to 1690 µScm^{-1}. The EC of SW for the 2nd survey ranged from 89 µScm^{-1} to 21,700 µScm^{-1} due to the presence of a sample from a saline lake (L3). However, the highest pH values measured in both types of water were quite similar (8.9 in both GW and SW for the 1st survey, and 9.3 and 9.7 in GW and SW, respectively, for the 2nd survey), the lowest measured pH values were found in groundwater samples, with the values of 6.1 and 5.9 (1st and 2nd surveys, respectively) in contrast to the 7.6 pH value measured in surface waters in both surveys. The redox potential (Eh) ranges from -287 to 224 mV (1st survey) and from -251 to 589 mV (2nd survey) in GW, whereas in SW ranges from 123 to 185 mV (1st survey) and from 113 to 201 mV (2nd survey). The most negative values of GW are attributable to the thermal spring ETH S5 rising from lake sediments close to Lake Langano.

In GW, fluoride concentrations vary from 0.1 to 68.9 mg L^{-1}, in the 1st survey, and from 0.1 to 68.2 mg L^{-1} in the 2nd survey, showing similar ranges in both cases, but with different average values (6,7 and 7,8 mg L^{-1} for the 1st and 2nd surveys, respectively). In SW the fluoride concentration ranges from 0.7 to 12.9 mg L^{-1} (1st survey) and from 0.6 to 244.2 mg L^{-1} (2nd survey). The wider range for the SW in the 2nd survey is due to the high value sampled on Lake Shala. The highest concentrations correspond to hydrothermal springs (samples S3, S5, and S9 with the concentrations of 68.9, 44.5, and 24.0 mg L^{-1}, respectively) and to the hand-dug well HW2 (34.0 mg L^{-1}).

Overall, higher fluoride concentrations have been detected along the rift floor, specifically in correspondence with lake sediments. Moving to the highland (towards both the eastern and western plateau), the fluoride concentration tends to decrease, as shown by the spatial distribution in Fig. 12.

In the study area, seasonal variations of fluoride content have been detected (Fig. 13). The F$^-$ concentrations tend to increase from the dry season (1st survey) to the period after the rainy season (2nd survey) in those samples from the area of the Central Main Ethiopian Rift (CMER), whereas it decreases in samples from the NMER area.

A positive F$^-$ trend has been highlighted with EC and, in some cases, with temperature (Fig. 14a and b). The EC tends to increase the movement towards the rift floor. An evident relationship can be observed regarding temperature for F$^-$ values below 4 mg L^{-1}; conversely, no apparent tendency is observed over this value.

As previously described, the NMER groundwater circulation is strongly influenced by the geological structures and has a higher time response to the CMER during the rainy season. This probably results in a dilution effect on the fluoride concentration, which decreases in the 2nd survey.

Multiple and concurrent factors, currently under investigation, can affect the dynamic fluoride contamination. Previous studies in the area (Ayenew, 2008; Rango et al., 2009 and 2010; Bretzler et al., 2011) showed that high fluoride contents are related to water hosted in acidic volcanic rocks, especially in ignimbrites, rhyolites, and pumice-cropping-out in the rift floor. The water/rock–sediment interaction, together with the weathering products of glass components, enriched groundwaters with major ions, and F$^-$. In this study, we found the same spatial water/rock type association (Fig. 12).

5. Conclusions

The complex set of all the studies carried out in the research area, i.e., the bibliographic, geological, stratigraphic, hydrogeological, hydrogeochemical, and geophysical studies, along with data strictly concerning water quality, allow us to formulate some important, but not definitive, conclusions. The synthesis of these studies is well represented by the combination of Figs. 8 to 12. The aquifers are recharged from rain, floodwaters, stream channel loss, or groundwater inflow from the mountains. The hydrogeological conceptual model shows a complex hydrogeological environment and an evident hydraulic interconnection between different aquifer units. Approximately 62 % of the analyzed water samples exceeded the WHO threshold of 1.5 mg L^{-1} for fluoride concentration in drinking water. The highest values were detected for the samples located in correspondence of lacustrine sediments and thermal water. A firm point of these conclusions is that all water points with acceptable fluoride content are systematically found in environments characterized by fractured ignimbrite outcrops, namely the Pliocene Nazret Group ignimbrites (see also Fig. 3). Aforementioned ignimbrites outcrop at the shoulders of the rift and tend to deepen towards the rift axis, except for some interesting outcrops in the downstream areas.

In this context, some observations must be made. First, the ignimbrites, which have thicknesses of the order of several hundred meters, lie on Oligocene–Miocene basalts that generally, in similar environments, have acceptable fluoride contents. This condition would exclude water contamination generated in depth, which has to be verified. If the last consideration is reliable, the contamination should originate from the surface and near surface materials, such as the Quaternary sediments of alluvial and lacustrine origin. To verify the above interpretation, the following questions need to be resolved: if the water fluoride contamination spread vertically from top to bottom, or if it can be assumed that the fluoride contamination is confined to the surface and the near-surface regions. Regardless of the in-depth study of the whole information already acquired, to answer the above question, it would be interesting and useful to drill at least two research wells, the first at an ignimbrite outcrop, downstream from the rift shoulders and the second at an area where outcropping materials are the Quaternary sediments, penetrating the underlying ignimbrites to verify the water quality. In purely
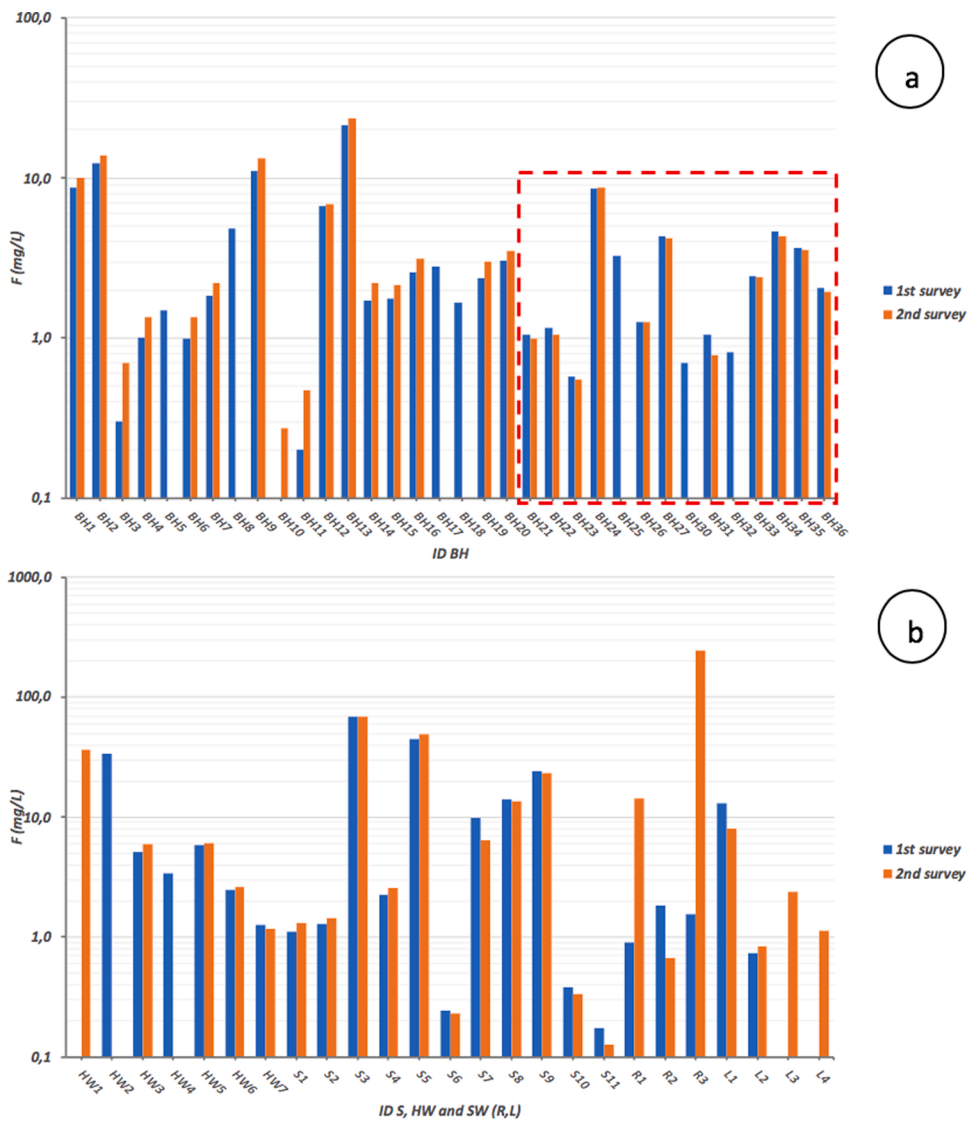
Fig. 13. Seasonal variation of fluoride concentration for the 1st (a) and 2nd (b) survey. BH: boreholes; HW: hand dug wells; S: springs; and SW: surface waters (R = rivers and L = lakes). Within the red dashed box, the samples of NMER.
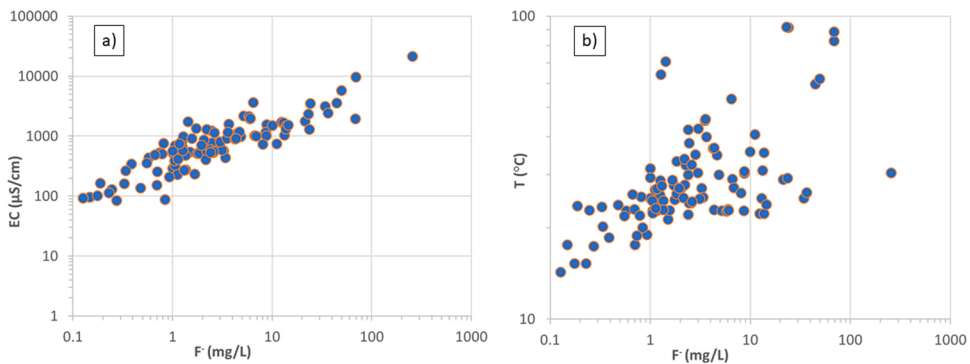
Fig. 14. Scatter diagram EC vs F⁻ concentration (a) and T vs F⁻ concentration (b) in water samples collected during the 1st and 2nd survey.

practical terms, it would also be advisable to accurately verify the conditions of one or more existing wells located in the ignimbrite outcroppings at the shoulders of the rift and, in the case of favorable outcomes, to design straightforward and economic hydraulic facilities to provide the resident populations in the downstream regions with water of acceptable quality. Moreover, ongoing tracer-based studies by the authors should emphasize groundwater age indicators (^{14}C, ^{3}H, ^{36}Cl) and tracers, such as sulfur and strontium isotopes, to better systematize the hydrogeology of the study area. Noticeably, the present dataset provides a basis for planning an effective groundwater management strategy to improve access to safe water. Nevertheless, such plans cannot be designed merely based on hydrogeological scientific and technical results, as other solutions such as the innovative defluoridation method, are effective for rural communities, and social and economic factors must also be considered (Idini et al., 2020).

Declaration of Competing Interest

The authors declare no conflict of interest.

Acknowledgments

Appendix A. Supplementary data

Supplementary material related to this article can be found, in the online version, at doi:https://doi.org/10.1016/j.ejrh.2020.100756.

References

Abebe, T., Manetti, P., Bonini, M., Corti, G., Innocenti, F., Mazzarini, F., Pecskay, Z., 2005. Geological Map (scale 1:200000) of the Northern Main Ethiopian Rift and Its Implication for the Volcano-tectonic Evolution of the Rift. Geological Society of America, Boulder Colorado, USA, Maps and Charts series, MCH094.

Abebe, B., Acocella, V., Korme, T., Ayalew, D., 2007. Quaternary faulting and volcanism in the main ethiopian rift. J. Afr. Earth Sci. 48 (2–3), 115–124. https://doi.org/10.1016/j.jafrearsci.2006.10.005.

Agostini, A., Bonini, M., Corti, G., Sani, F., Manetti, P., 2011. Distribution of quaternary deformation in the central main ethiopian rift, East Africa. Tectonics 30. https://doi.org/10.1029/2010TC002833.

Alemayehu, T., 2010. Groundwater dynamics in the East African rift system. In: Xu, Y., Braune, E. (Eds.), "Sustainable Groundwater Resources in Africa. CRC Press, Taylor and Francis, pp. 93–106. https://doi.org/10.1201/9780203859452.

Alemayehu, T., Ayenew, T., Kebede, S., 2006. Hydrogeochemical and lake level changes in the Ethiopian Rift. Jour. of Hydrology 316, 290–300. https://doi.org/10.1016/j.jhydrol.2005.04.024.

Ayenew, T., 2008. The distribution and hydrogeological controls of fluoride in the groundwater of central Ethiopian rift and adjacent highlands. Environmental Geology 54.6, pp. 1313–1324. https://doi.org/10.1007/s00254-007-0914-4. ISSN: 1432-0495. DOI: 10.1007/s00254- 007- 0914- 4. URL.

Azagegn, T., Asrat, A., Ayenew, T., Kebede, T., 2015. Litho-structural control on interbasin groundwater transfer in central Ethiopia. J. Afr. Earth Sci. 101, 383–395. https://doi.org/10.1016/j.jafrearsci.2014.10.008.

Boccaletti, M., Mazzuoli, R., Bonini, M., Trua, T., Abebe, B., 1999. Plio-Quaternary volcanotectonic activity in the northern sector of the Main Ethiopian Rift: relationships with oblique rifting. J. Afr. Earth Sci. 29 (4), 679–698. https://doi.org/10.1016/S0899-5362(99)00124-4. ISSN 1464-343X.

Bretzler, A., Osenbrück, K., Gloaguen, R., Ruprecht, J.S., Kebede, S., Stadler, S., 2011. Groundwater origin and flow dynamics in active rift systems - A multi-isotope approach in the Main Ethiopian Rift. J. Hydrol. 402 (3–4), 274–289. https://doi.org/10.1016/j.jhydrol.201110.1016/j.jhydrol.2011.03.022.03.022.

Butscher, C., Scheidler, S., Farhadian, H., Dresmann, H., Huggenberger, P., 2017. Swelling potential of clay-sulfate rocks in tunneling in complex geological settings and impact of hydraulic measures assessed by 3D groundwater modeling. Eng. Geol. 221, 143–153. https://doi.org/10.1016/j.enggeo.2017.03.010.

Corti, G., 2009. Continental rift evolution: from rift initiation to incipient break-up in the Main Ethiopian Rift, East Africa. Earth Sci. Rev. 96, 1–53. https://doi.org/10.1016/j.earscirev.2009.06.005.

Corti, G., 2012. Evolution and characteristics of continental rifting: analog modeling-inspired view and comparison with examples from the East African Rift System. Tectonophysics 522–523, 1–33. https://doi.org/10.1016/j.tecto.2011.06.010.

Davidson, A., Rex, D.C., 1980. Age of volcanism and rifting in southwestern Ethiopia. Nature 283, 657–658.

Davies, J., 2008. The benefits of a scientific approach to sustainable development of groundwater. Applied Groundwater Studies in Africa, IAH Selected Papers Ol 13. ISBN 978-0-415-45273-1, 85-101.

Delcamp, A., Roberti, G., van Wyk de Vries, B., 2016. Water in volcanoes: evolution, storage and rapid release during landslides. Bull. Volcanol. 78 https://doi.org/10.1007/s00445-016-1082-8.

Fentaw, B., Mihret, M., 2011. Hydrogeological map of Akaki–Beseka 1:250.000 scale (Ethiopia), sheet NC 37-14. Geological Survey of Ethiopia. Ministry of Mines.

Ghiglieri, G., Carletti, A., 2010. Integrated approach to choosing suitable areas for the realization of productive wells in rural areas of sub-Saharan Africa. Hydrol. Sci. J. Des Sci. Hydrol. 55 (8), 1357–1370. https://doi.org/10.1080/02626667.2010.527845.

Ghiglieri, G., Balia, R., Oggiano, G., Pittalis, D., 2010. Prospecting for safe (low fluoride) groundwater in the Eastern African Rift: the Arumeru District (Northern Tanzania). Hydrol. Earth Syst. Sci. Discuss. 14, 1081–1091. https://doi.org/10.5194/hess-14-1081-2010.

Ghiglieri, G., Pittalis, D., Cerri, G., Oggiano, G., 2012. Hydrogeology and hydrogeochemistry of an alkaline volcanic area: The NE Mt. Meru slope (East African Rift-Northern Tanzania). Hydrol. Earth Syst. Sci. Discuss. 16, 529–541. https://doi.org/10.5194/hess-16-529-2012.

Ghiglieri, G., Carletti, A., Da Pelo, S., Cocco, F., Funedda, A., Loi, A., Manta, F., Pittalis, D., 2016. Three-dimensional hydrogeological reconstruction based on geological depositional model: a case study from the coastal plain of Arborea (Sardinia, Italy). Eng. Geol. 207, 103–114. https://doi.org/10.1016/j.enggeo.2016.04.014.

Idini, A., Frau, F., Gutierrez, L., Dore, E., Nocella, G., Ghiglieri, G., 2020. Application of octacalcium phosphate with an innovative household-scale defluoridator prototype and behavioral determinants of its adoption in rural communities of the East African Rift Valley". Integr. Environ. Assess. Manag. 2020, 15. https://doi.org/10.1002/ieam.4262 accepted on 6 March 2020.

JMP, 2004. Global Water Supply and Sanitation 2004 Report. Joint monitoring programme WHO/UNICEF, World Health Organization, Geneva.

Kebede, S., Travi, Y., Alemayehu, T., Ayenew, T., Tessema, Z., 2008. Groundwater origin and flow along selected transects in Ethiopian Rift volcanic aquifer. Hydrogeol. J. 16, 55–73. https://doi.org/10.1007/s10040-007-0210-0.

MacDonald, A.M., Davies, J., Calow, R.C., 2008. African hydrogeology and rural water supply. In: - Applied Groundwater Studies in Africa – IAH Selected Papers, Vol 13, pp. 127–148. ISBN 978-0-415-45273-1.

Mckenzie, J.M., Mark, B.G., Thompson, L.G., Schotterer, U., Lin, P.-N., 2010. A hydrogeochemical survey of Kilimanjaro (Tanzania): implications for water sources and ages. Hydrogeol. J. 18, 985–995. https://doi.org/10.1007/s10040-009-0558-4.

Pietersen, K., 2005. Groundwater crucial to rural development. The Water Wheel March/April 2005. Water Research Commission, Pretoria.

Rango, T., Bianchini, G., Beccaluva, L., Ayenew, T., Colombani, N., 2009. Hydrogeochemical study in the Main Ethiopian Rift: new insights to the source and enrichment mechanism of fluoride. Environ. Geol. 58, 109–118. https://doi.org/10.1007/s00254-008-1498-3.

Rango, T., Bianchini, G., Beccaluva, L., Tassinari, R., 2010. Geochemistry and water quality assessment of central Main Ethiopian Rift natural waters with emphasis on source and occurrence of fluoride and arsenic. J. Afr. Earth Sci. 57, 479–491. https://doi.org/10.1016/j.jafrearsci.2009.12.005.

Tam, V.T., Batelaan, O., Le, T.T., Nhan, P.Q., 2014. Three-dimensional hydrostratigraphical modelling to support evaluation of recharge and saltwater intrusion in a coastal groundwater system in Vietnam. Hydrogeol. J. 22 (8), 1749–1762. https://doi.org/10.1007/s10040-014-1185-2.

Trippanera, D., Acocella, V., Ruch, J., Abebe, B., 2015. Fault and graben growth along active magmatic divergent plate boundaries in Iceland and Ethiopia. Tectonics 34 (11), 2318–2348. https://doi.org/10.1002/2015TC003991.

Wolde Gabriel, G., Aronson, J., Walter, R.C., 1990. Tectonic development of the Main Ethiopian rift. Geol. Soc. Am. Bull. 102, 439–458.

Wolfenden, E., Ebinger, C., Yirgu, G., Deino, A., Ayalew, D., 2004. Evolution of the northern Main Ethiopian rift: birth of a triple junction. Earth Planet. Sci. Lett. 224 (1–2), 213–228. https://doi.org/10.1016/j.epsl.2004.04.022.

Xue, Y., Sun, M., Ma, A., 2004. On the reconstruction of three-dimensional complex geological objects using Delaunay triangulation. Future Gener. Comput. Syst. 20, 1227–1234. https://doi.org/10.1016/j.future.2003.11.012.